Chinese Chemical Letters 31 (2020) 1004–1008

Contents lists available at ScienceDirect

Chinese Chemical Letters

journal homepage: www.elsevier.com/locate/cclet

Communication

Porous and free-standing $Ti_3C_2T_x$-RGO film with ultrahigh gravimetric capacitance for supercapacitors

Yongzheng Fang[a,1], Bowen Yang[a,1], Dongtong He[a], Huipeng Li[a], Kai Zhu[a,c,*], Lin Wu[b,**], Ke Ye[a], Kui Cheng[a], Jun Yan[a], Guiling Wang[a], Dianxue Cao[a,*]

[a] Key Laboratory of Superlight Materials and Surface Technology, Ministry of Education, College of Material Science and Chemical Engineering, Harbin Engineering University, Harbin 150001, China
[b] Teachers Education College of Harbin Normal University, Harbin 150001, China
[c] Key Laboratory of Advanced Chemical Power Sources, Guizhou Meiling Power Sources Co., Ltd., Zunyi 563003, China

ARTICLE INFO

Article history:
Received 29 July 2019
Received in revised form 15 August 2019
Accepted 19 August 2019
Available online 26 August 2019

Keywords:
MXene
RGO
Cross-linked porous
Supercapacitors
High capacitance
Thickness independent

ABSTRACT

MXene-based electrode materials exhibit favorable supercapacitor performance in sulfuric acid due to praised pseudocapacitance charge storage mechanism. However, self-stacking of conventional MXene electrodes severely restricts their electrochemical performance, especially at high loading. Herein, a flexible cross-linked porous $Ti_3C_2T_x$-MXene-reduced graphene oxide ($Ti_3C_2T_x$-RGO) film is skillfully designed and synthesized by microscopic explosion of graphene oxide (GO) at sudden high temperature. The generated chamber structure between layers could hold a few of electrolyte, leading to a close-fitting reaction at interlayer and avoiding complex ions transmission paths. The $Ti_3C_2T_x$-RGO film displayed a preferable rate performance than that of pure $Ti_3C_2T_x$ film and a high capacitance of 505 F/g at 2 mV/s. Furthermore, the uniform intralayer structure and unique energy storage process lead to thickness-independenct electrochemical performances. This work provides a simple and feasible improvement approach for the design of MXene-based electrodes, which can be spread other electrochemical systems limited by ions transport, such as metal ions batteries and catalysis.

Supercapacitors have been regarded as one of promising representative energy storage devices with high-power density due to their unique advantages such as a long cycle life and environmental friendliness [1]. Usually, supercapacitors are classified into two categories based on charge storage mechanism of electrode materials. One is typical electrical double-layer capacitors (EDLCs), which storages charges through adsorbing/desorbing process at the electrode/electrolyte interface [2]. Although EDLCs provide a stable cycling performance, their low capacitance
cannot meet increasing requirement of high-energy devices. Pseudocapacitors, as another type supercapacitor, permit fast redox reaction on materials surface layer, engendering larger energy density due to more charges transfer [3]. Thus, pseudocapacitors become a promising candidate that can offer not only high power density but also capable energy density for power equipment. However, traditional pseudocapacitors electrode materials such as RuO_2 [4], MnO_2 [5–9], V_2O_5 [10,11] are confronted with many problems such as high price, low electrical conductivity, and poor cycling performance [12]. Thus, it is necessary to explore capable electrode materials for pseudocapacitors.

MXene, an emerging group of two-dimensional (2D) materials, have present their potential as electrochemical energy storage materials with high energy and power densities due to the large surface to volume ratios, high conductivity, rich exposed active site, and lack of bulk phase diffusion [13,14]. Usually, MXene is prepared by selective etching of the most lively "A" atoms layer from the layered transition metal carbides (MAX) by using the synthetic hydrofluoric acid solution (LiF and HCl), which results in

* Corresponding author at: Key Laboratory of Superlight Materials and Surface Technology, Ministry of Education, College of Material Science and Chemical Engineering, Harbin Engineering University, Harbin 150001, China.
** Corresponding author at: Teachers Education College of Harbin Normal University, Harbin, 150001, China.
E-mail addresses: kzhu@hrbeu.edu.cn (K. Zhu), hsdhxwulin@163.com (L. Wu), caodianxue@hrbeu.edu.cn (D. Cao).
[1] These authors contributed equally to this work.

https://doi.org/10.1016/j.cclet.2019.08.043
1001-8417/

abundant of surface functional groups (−OH, −F and −O) [15,16]. The surface functional groups provide hydrophilicity and a large number of active sites [17]. Recently, Gogotsi's group demonstrated the pseudocapacitance charge storage mechanism of MXene in H_2SO_4 electrolyte. The Ti oxidation state and deprotonation/protonation of −O function groups change with the stripping/plating processes of H^+, leading to a large capacitance [2,18]. However, similar to other 2D materials, when MXene nanosheets are fabricated into electrodes, they suffer from the self-restacking problem due to van der Waals force between layers, resulting in a covered reaction sites and tortuous ions transmission path [15]. Recently, constructing a 3D electrode becomes an effective strategy to enhance the electrochemical performance [19]. R. Lukatskaya *et al.* synthesized a macroporous MXene film by using polymethyl methacrylate as a template to construct a 3D film electrode, which deliver up to 310 F/g [2]. Xia *et al.* realized the vertical alignment of MXene by mechanically shearing of a discotic lamellar liquid-crystal phase of $Ti_3C_2T_x$ and a capacitance of 275 F/g was obtained [13]. These strategies realized short vertical transmission paths, resulting in a favorable rate performance. Unfortunately, the complex and demanding preparation processes limit their large-scale production and application.

Herein, we designed and prepared a porous MXene-RGO flexible film by a self-puffing reaction of MXene-GO film. The sparking reaction of GO created a large amount of cross-linked porous structure between the MXene layers. As-prepared MXene-RGO film was employed as electrode directly without addition of heavy metal current collector and inactive binder. RGO successfully prevents the self-restacking of MXene and the chamber structure between layers can accommodate a little of electrolyte, which causes a close-fitting reaction, avoiding complex ions transmission paths and promising fast ion storage behaviors. Therefore, the MXene-RGO films displayed a large capacitance, remarkable rate ability and stable cycling performance. Moreover, such a unique chamber structure made the capacitance was less affected by thickness of electrode and loading of active materials.

Fig. 1a displays schematic illustration of fabrication process of the $Ti_3C_2T_x$-RGO film with an interlayer link-cross porous structure. Firstly, the uniform mixture of few-layered $Ti_3C_2T_x$ and GO nanosheets was transformed into the compact $Ti_3C_2T_x$-GO film through vacuum filtration. Then, $Ti_3C_2T_x$-GO film touched a hot-table and a micro-explosion reaction occurred. Due to abrupt and larger heat, GO was reduced into RGO. During oxygen-containing groups removal process, generated gas enlarged the interlayer spacing and created a cross-linked porous structure [20]. Finally, $Ti_3C_2T_x$-RGO flexible film was obtained. In such a porous structure, H_2SO_4 electrolyte will infuse the nano-chambers among layers due to the hydrophilic surface of $Ti_3C_2T_x$ as shown in Fig. 1b [21]. During the discharging and charging electrochemical reaction, the H^+ will move toward $Ti_3C_2T_x$ surface/interlayer, and back into the chamber, respectively. Such a close-fitting reaction can accelerate the ions transport. Different with the lengthy and tortuous H^+ transmission path in traditional multilayer $Ti_3C_2T_x$ films, such reaction process achieves ultra-fast ions storage behavior. In addition, the porous structure prepared by micro-explosion makes $Ti_3C_2T_x$ separate from each other, which enables single layer or a few layers of $Ti_3C_2T_x$ participate in the reaction at each nanoelectrode between the layers, increasing electrochemical utilization. Fig. 1c shows the images of $Ti_3C_2T_x$-GO and $Ti_3C_2T_x$-RGO films. $Ti_3C_2T_x$-GO film shows a black and smooth surface. After micro-explosion, the $Ti_3C_2T_x$-RGO film presented gray and pleated surface due to reducing process and increased interlayer spacing. Meanwhile, $Ti_3C_2T_x$-RGO film displayed a good flexibility.

The microscopic morphologies of the $Ti_3C_2T_x$-GO and $Ti_3C_2T_x$-RGO films were observed by a scanning electron microscopy (SEM). Figs. 2a and b exhibit a tightly stacked structure for $Ti_3C_2T_x$-GO film, and Figs. 2c and d display a cross-linked and porous structure in the $Ti_3C_2T_x$-RGO interlayer after micro-explosion. It is noteworthy that the layer spacing is enlarged and the chamber height ranges from 100 nm to 1 μm, implying that a few of electrolyte can be stored between layers. X-ray diffractometer (XRD) was employed to investigate crystal structure changes from Ti_3AlC_2 to $Ti_3C_2T_x$ and from $Ti_3C_2T_x$-GO to $Ti_3C_2T_x$-RGO. As shown in Fig. S1 (Supporting information), the highest peak at 39.5° of Ti_3AlC_2 was completely obliterated and the (002) characteristic peak of $Ti_3C_2T_x$ before 10° occurred after etching and ultrasound process, suggesting successful synthesis of $Ti_3C_2T_x$ MXene [3]. For the $Ti_3C_2T_x$-GO film, the (002) peak strength weakened and moved 0.6° to the left due to the introduction of GO and increased interlayer spacing, which is similar to Yan's report [15]. After the reduction process, (002) peak of the $Ti_3C_2T_x$-RGO film became very wide and flat, which can be attributed to enlarged layer spacings and different orientations for $Ti_3C_2T_x$ nanosheets (Fig. 2e) [22]. In order to investigate the functional groups on the film surface before and after the micro-explosion, X-ray photoemission spectroscopy (XPS) was performed. The C 1s spectra as shown in Fig. 2f indicated the existence of lots of oxygen-containing groups on $Ti_3C_2T_x$-GO film, with the peaks at 284.0, 284.6, 285.6, 286.7 and 288.2 eV correspond to C=C, C—C, C—OH, C–O and C=O bonds, respectively [23]. After the micro-explosion, a large proportion of function groups were removed, which can be attributed to the reduction process from GO to RGO (Fig. 2g). In contrast, from Ti 2p (Fig. S2 in Supporting information) and F 1s (Fig. S3 in Supporting information) spectra, $Ti_3C_2T_x$ surface functional groups had almost

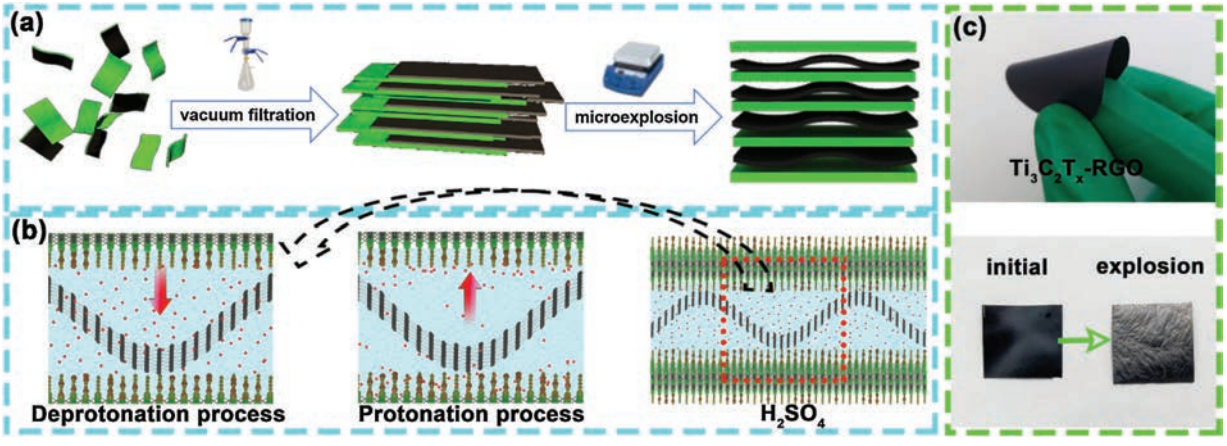

Fig. 1. (a) Synthetic schematic for $Ti_3C_2T_x$-RGO film; (b) Reaction mechanism for $Ti_3C_2T_x$-RGO in H_2SO_4 electrolyte; (c) Physical pictures for $Ti_3C_2T_x$-GO and $Ti_3C_2T_x$-RGO films.

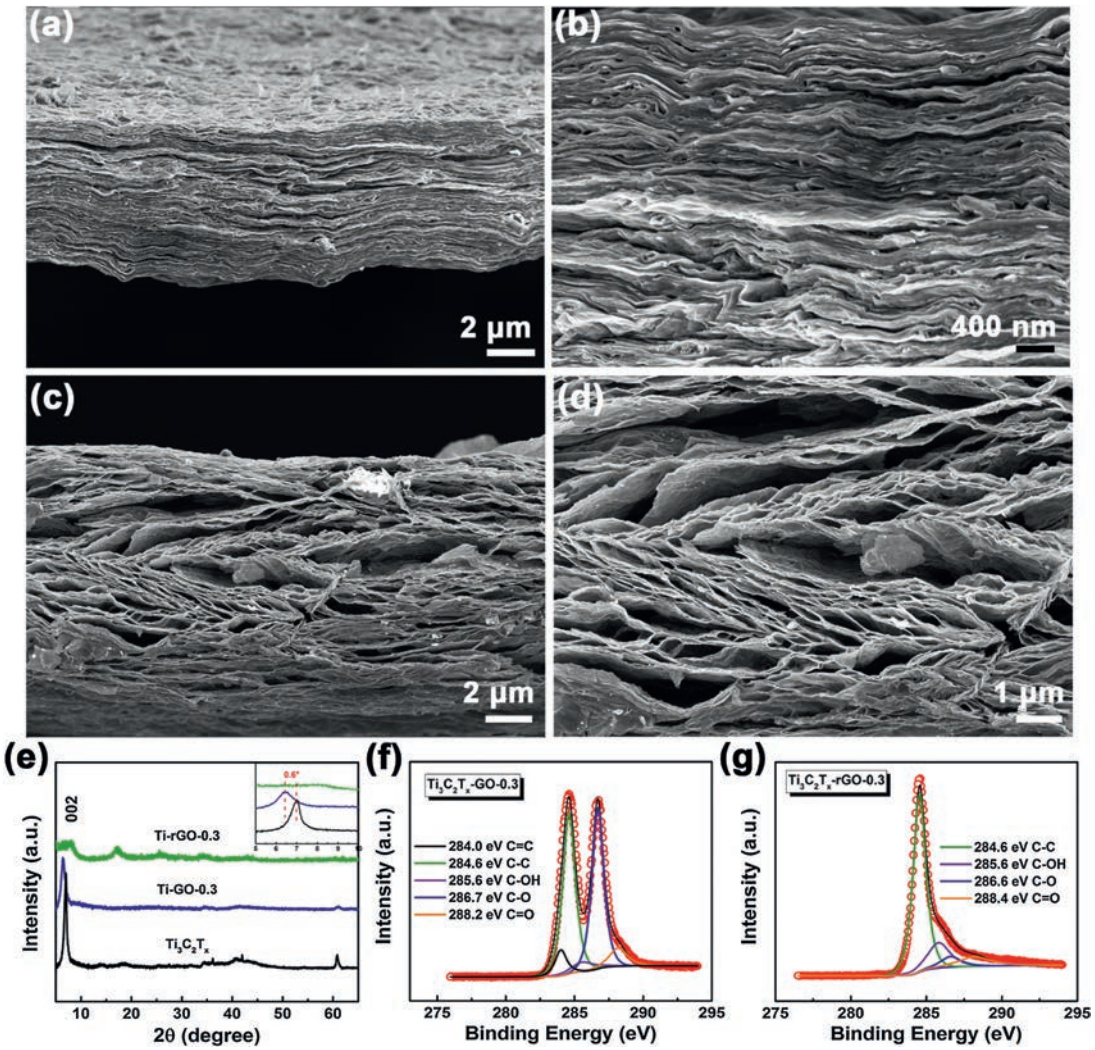

Fig. 2. (a–d) Microscopic morphology and (e) XRD before and after micro-explosion reaction of $Ti_3C_2T_x$-GO films; XPS for (f) $Ti_3C_2T_x$-GO and (g) $Ti_3C_2T_x$-RGO.

no change, suggesting stable functional groups and stronger binding energy between Ti_3C_2 and T_x. The generated RGO enhance electronic conductivity and remained functional groups ensure the hydrophilicity, promising the fast penetration of electrolyte.

Electrochemical performance of $Ti_3C_2T_x$-RGO freestanding electrode was evaluated in a three-electrode system with carbon-point as a counter electrode and Ag/AgCl as a reference electrode in 3 mol/L H_2SO_4 electrolyte. The detailed experimental method is provided in supporting information. To investigate the synergy effect between $Ti_3C_2T_x$ and RGO, and their optimized mass ratio, five samples were designed and prepared with the same quality (Table 1).

Fig. 3a shows the cyclic voltammetry (CV) curves of pure $Ti_3C_2T_x$ and $Ti_3C_2T_x$-RGO films at the scan rate of 20 mV/s. When the content of GO is little, $Ti_3C_2T_x$-RGO-0.1 films exhibit smaller integral area, which can be attributed to a smaller layer spacing variation. When the content of GO is nimiety, the smallest area was obtained for $Ti_3C_2T_x$-RGO-0.4 without redox peaks, due to low capacitance and conductivity of RGO. In contrast, $Ti_3C_2T_x$-RGO-0.2 and $Ti_3C_2T_x$-RGO-0.3 films display larger area than the pure $Ti_3C_2T_x$, and a couple of redox peaks locate at −0.3 V and −0.45 V (*vs.* Ag/AgCl) represent a reversible pseudocapacitance reaction associated with the deprotonation/protonation process of functional groups and the change of Ti oxidation state. The CV curves of these at different scan rates are shown in Fig. 3c and Fig. S4 (Supporting information). $Ti_3C_2T_x$-RGO-0.3 film kept the shape best, suggesting the outstanding rate ability. The specific capacitance was calculated from the CV curves as shown in Fig. 3b. At 2 mV/s, the $Ti_3C_2T_x$-RGO-0.3 showed the highest capacity of 505 F/g (808 F/cm^2), among $Ti_3C_2T_x$-RGO-0.2 (452 F/g), $Ti_3C_2T_x$ (436 F/g), $Ti_3C_2T_x$-RGO-0.1 (433 F/g) and $Ti_3C_2T_x$-RGO-0.4 (373 F/g) samples. Even at 100 mV/s, $Ti_3C_2T_x$-RGO-0.3 still maintained a high

Table 1
Samples composition and number of $Ti_3C_2T_x$-RGO films.

Samples	$Ti_3C_2T_x$-RGO-0	$Ti_3C_2T_x$-RGO-0.1	$Ti_3C_2T_x$-RGO-0.2	$Ti_3C_2T_x$-RGO-0.3	$Ti_3C_2T_x$-RGO-0.4
$Ti_3C_2T_x$ (wt%)	100	90	80	70	60
GO (wt%)	0	10	20	30	40
Total mass (mg)	20	20	20	20	20

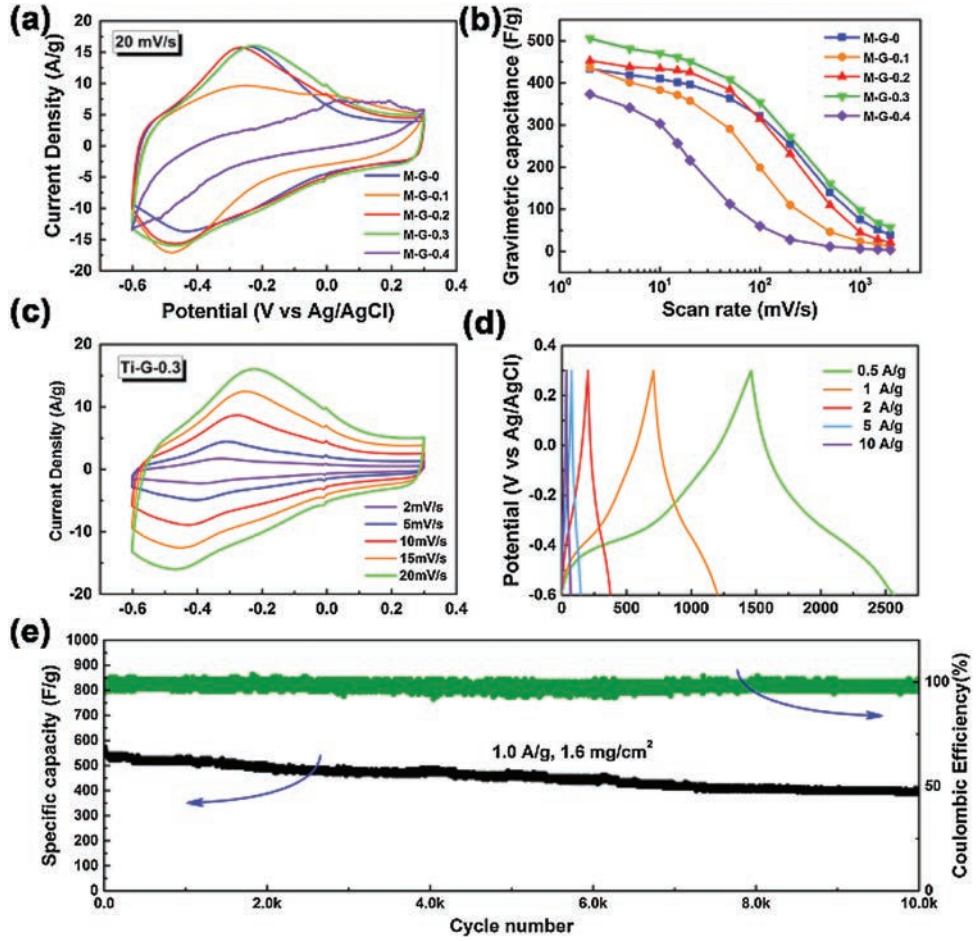

Fig. 3. Electrochemical performance for $Ti_3C_2T_x$-RGO films in 3 mol/L H_2SO_4 electrolyte. (a) CV curves at 20 mV/s and (b) gravimetric capacitances at different scan rates of different $Ti_3C_2T_x$-RGO films; (c) CV curves, (d) charge-discharge curves and (e) cycling performance of $Ti_3C_2T_x$-RGO-0.3 film.

capacity of 353 F/g (564.8 F/cm^2). It suggests that the optimal ratio of $Ti_3C_2T_x$:GO is 7:3. It should be noticed that the gravimetric capacitance of 505 F/g (561 C/g in the voltage window of 0.9 V) is closed to its theoretical value (615 C/g) reported by Yury's group [2]. Such a result is competitive with previous excellent reports is shown in Table S1 (Supporting information). $Ti_3C_2T_x$-RGO-0.3 film

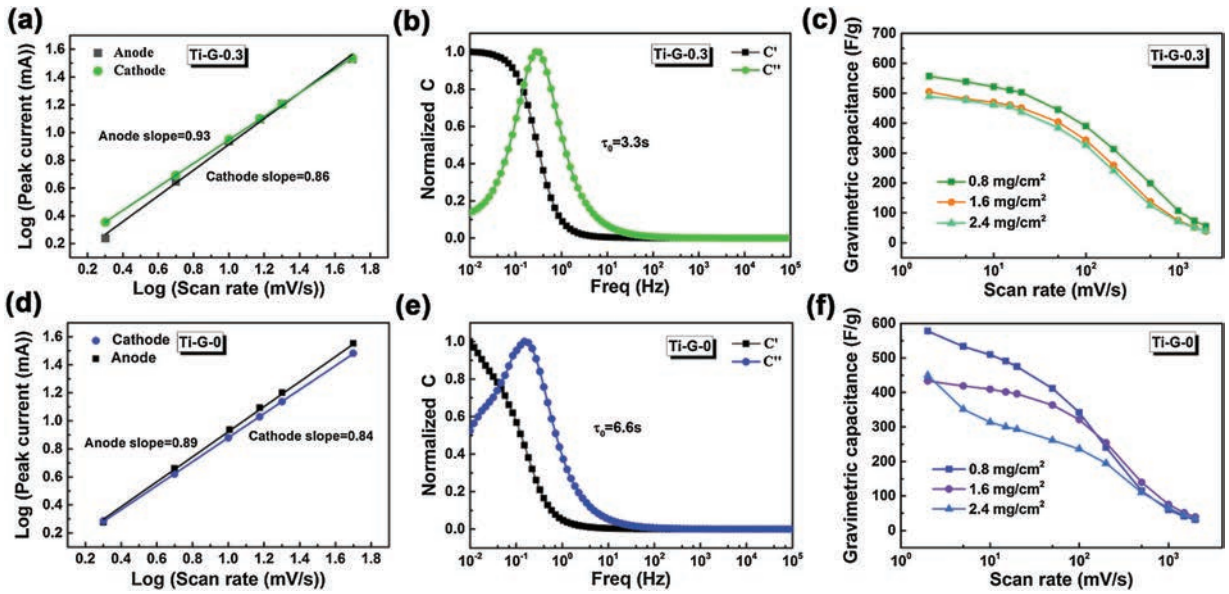

Fig. 4. Performance comparison between $Ti_3C_2T_x$-RGO-0.3 (up) and pure $Ti_3C_2T_x$ films (below). (a, d) The relationship between peak currents and scan rates from 2 mV/s to 50 mV/s; (b, e) Normalized real and imaginary capacitances; (c, f) Gravimetric capacitances of different surface loads in at different scan rates.

exhibits the nonlinear galvanostatic charge/discharge curves with a couple of charge/discharge platforms corresponding to redox peaks in the CV curves (Fig. 3d). The discharge specific capacitance was calculated to be up to 612 F/g at 0.5 A/g, followed by 505, 386, 385 and 371 F/g at 1.0, 2.0, 5.0 and 10 A/g, respectively. In addition, $Ti_3C_2T_x$-RGO-0.3 presents an excellent cycling performance at 1.0 A/g as shown in Fig. 3e, corresponding to the decay of only 0.0071% per cycle. In order to certify the practical application value, an asymmetric supercapacitor was assembled with the $Ti_3C_2T_x$-RGO-0.3 as a cathode and active carbon (AC) as an anode. The electrochemical performance was performed in 01.0 V as shown the Fig. S5 (Supporting information). Stable CV curves indicate a good dynamic match for cathode and anode. A pair of slight redox peaks (0.6 V and 0.5 V) can be observed and classified as a Faraday reaction of $Ti_3C_2T_x$.

To further understand electrochemical dynamics of $Ti_3C_2T_x$-RGO-0.3 film, the mechanism of electrochemical process was investigated. In the CV curves, the peak current (i) and scan rate (v) obey the relationship as follow:

$$i = av^b \tag{1}$$

in which the a and b are the constant and b-value is between 0.5 to 1.0. When the electrochemical process controlled by diffusion behavior, the b-value is close to 0.5, while the b-value of 1.0 represents a fast reaction without diffusion-controlled [24,25]. As shown in Fig. 4a, the b-values of $Ti_3C_2T_x$-RGO-0.3 electrode are 0.86 and 0.93 for cathodic and anodic peaks, respectively. In contrast, the lower b-values of 0.84 and 0.89 of pure $Ti_3C_2T_x$ film as shown in Fig. 4d indicate a slower reaction rate due to the longer transmission path of H^+ in the tightly stacked layers. While the modified electrode structure makes a close-fitting electrochemical reaction, that is, interlayer MXene reacts directly with H^+ in the interlayer pores, avoiding longer transport. In order to further certify that, the impedance spectroscopy of they were studied through a complex model capacitance as follow:

$$C'(\omega) = \frac{-Z''(\omega)}{\omega||Z(\omega)||^2} \tag{2}$$

$$C''(\omega) = \frac{Z'(\omega)}{\omega||Z(\omega)||^2} \tag{3}$$

in which, the $z'(\omega)$, $z''(\omega)$, and ω represent real, imaginary parts, and angular frequency of the complex impedance, respectively; while the $C'(\omega)$ and $C''(\omega)$ are the real and imaginary parts for the complex capacitances [24]. As shown in Figs. 4b and e, the $C'(\omega)$ decreases slower with the frequency for $Ti_3C_2T_x$-RGO-0.3 electrode, suggesting faster diffusion and reaction rate of ions. In addition, the minimal characteristic relaxation time constant τ_0 (the minimum time required to release all energy when the efficiency is greater than 50%) can be calculated by the characteristic frequency f_0, corresponding to the half value of C' and the highest value of C'' [15]. Half of the time (3.3 s) of MXene-RGO-0.3 electrodes was obtained compared to the pure MXene (6.6 s). The above results demonstrate the faster reaction dynamics for the porous MXene-RGO-0.3 film. Moreover, on account of the uniform intralayer structure, $Ti_3C_2T_x$-RGO film will get rid of the surface loading limit, which is an affliction in traditional tight stacked film. As shown in Fig. 4f, the specific capacitance of pure $Ti_3C_2T_x$ film decreases sharply with increasing surface loading. In contrast, $Ti_3C_2T_x$-RGO-0.3 presents a good rate performance independent of the mass loading (Fig. 4c), which is very industrially significant for obtaining high-energy electrochemical devices.

In summary, a flexible cross-linked porous $Ti_3C_2T_x$-RGO film was prepared through a micro-explosion reaction, which prevented the self-restacking of MXene, increased interlayer spacing obviously and exposed a large number of electrochemical active sites. Furthermore, the chamber structure between layer could accommodate a few of electrolyte, achieving a close-fitting reaction and avoiding lengthy transmission paths of active ions. As-prepared $Ti_3C_2T_x$-RGO-0.3 film exhibited a high rate performance and ultra-high gravimetric capacitance of 505 F/g at 2 mV/s and 353 F/g at 100 mV/s in the 3 mol/L H_2SO_4 electrolyte. Meanwhile, it also displayed excellent cycling stability. In addition, the unique close-fitting reaction and uniform intralayer structure promised the electrochemical performance of $Ti_3C_2T_x$-RGO film is less effect by mass loading than pure $Ti_3C_2T_x$ film. This work paved a way for the design and development of capable electrochemical energy storage devices with high mass loading of active materials.

Acknowledgments

This work was supported by the National Natural Science Foundation of China (Nos. 51702063, 51672056), Natural Science Foundation of Heilongjiang Province (No. LC2018004), China Postdoctoral Science Foundation (Nos. 2018M630340, 2019T120254) and the Fundamental Research Funds for the Central University (No. 3072019CF1006). The authors also thank the support from the Starting Research Fund from Harbin Normal University (No. XKB201420).

Appendix A. Supplementary data

Supplementary material related to this article can be found, in the online version, at doi:https://doi.org/10.1016/j.cclet.2019.08.043.

References

[1] Y. Wang, Y. Song, Y. Xia, Chem. Soc. Rev. 45 (2016) 5925–5950.
[2] M.R. Lukatskaya, S. Kota, Z. Lin, et al., Nat. Energy 2 (2017) 17105.
[3] M. Boota, Y. Gogotsi, Adv. Energy Mat. 9 (2019) 1802917.
[4] Q. Jiang, N. Kurra, M. Alhabeb, Y. Gogotsi, H.N. Alshareef, Adv. Energy Mater. 8 (2018) 1703043.
[5] X. Zhang, P. Yu, H. Zhang, et al., Electrochim. Acta 89 (2013) 523–529.
[6] X. Zhang, X. Sun, H. Zhang, D. Zhang, Y. Ma, Electrochim. Acta 87 (2013) 637–644.
[7] X. Zhang, X. Sun, H. Zhang, C. Li, Y. Ma, Electrochim. Acta 132 (2014) 315–322.
[8] J. Qin, Z.S. Wu, F. Zhou, et al., Chin. Chem. Lett. 29 (2018) 582–586.
[9] Y. Chen, C. Chen, R. Lv, et al., Chin. Chem. Lett. 29 (2018) 616–619.
[10] F. Liu, Z. Chen, G. Fang, et al., Nano-Micro Lett. 11 (2019) 25.
[11] Y. Yang, Y. Tang, G. Fang, et al., Energy Environ. Sci. 11 (2018) 3157–3162.
[12] C. Wang, P. Sun, G. Qu, J. Yin, X. Xu, Chin. Chem. Lett. 29 (2018) 1731–1740.
[13] Y. Xia, T.S. Mathis, M.Q. Zhao, et al., Nature 557 (2018) 409–412.
[14] K. Zhu, Y. Jin, F. Du, et al., J. Energy Chem. 31 (2019) 11–18.
[15] J. Yan, C.E. Ren, K. Maleski, et al., Adv. Funct. Mater. 27 (2017) 1701264.
[16] Q. Shan, X. Mu, M. Alhabeb, et al., Electrochem. Commun. 96 (2018) 103–107.
[17] S. Zhao, X. Meng, K. Zhu, et al., Energy Storage Mater. 8 (2017) 42–48.
[18] M. Hu, Z. Li, T. Hu, et al., ACS Nano 10 (2016) 11344–11350.
[19] X. Liu, R. Zhang, W. Yu, et al., Energy Storage Mater. 11 (2018) 83–90.
[20] D. Lin, Y. Liu, Z. Liang, et al., Nat. Nanotechnol. 11 (2016) 626.
[21] Z. Ma, K. Wang, Y. Qiu, et al., Energy 143 (2018) 43–55.
[22] M.Q. Zhao, X. Xie, C.E. Ren, et al., Adv. Mater. 29 (2017) 1702410.
[23] H. Hu, Z. Zhao, W. Wan, Y. Gogotsi, J. Qiu, Adv. Mater. 25 (2013) 2219–2223.
[24] Y. Fang, R. Hu, B. Liu, et al., J. Mater. Chem. 7 (2019) 5363–5372.
[25] Y. Luan, R. Hu, Y. Fang, et al., Nano-Micro Lett. 11 (2019) 30.